*J. Fluid Mech.* (1989), *vol.* 204, *pp.* 501–522
*Printed in Great Britain*



# The flow downstream of screens and its influence on the flow in the stagnation region of cylindrical bodies

By J. BÖTTCHER AND E. WEDEMEYER
DFVLR, Institute for Experimental Fluid Mechanics, Göttingen, FRG

(Received 30 October 1987 and in revised form 28 November 1988)

Screens used in the settling chamber of wind tunnels are known to introduce non-uniformities into the flow which, in turn, may influence the flow in the working section. A thorough investigation was made, using a flow visualization technique, of the development of non-uniformities generated by screens and their influence on the flow in the stagnation region of circular cylinders placed normal to the flow. A theoretical model of the flow downstream of screens is presented that is consistent with the experimental findings.

## 1. Introduction

Screens are used in the settling chamber of wind tunnels in order to reduce non-uniformities of the flow and to damp the oncoming turbulence. These favourable effects of screens have been studied extensively and reviews on this subject are given by Corrsin (1963) and Laws & Livesey (1978). On the other hand, screens introduce their own non-uniformities into the flow. Bohl (1940), Corrsin (1944), Baines & Peterson (1951) Morgan (1960), Bradshaw (1965) and de Bray (1967) describe non-uniformities of the flow downstream of screens and grids of parallel rods. Bohl (1940) and Corrsin (1944) have observed that the single jets emerging from the open parts of grids coalesce into groups to generate velocity variations of rather large scale.

Bradshaw (1965), de Bray (1967), Furuya & Osaka (1975) report about spanwise variations of surface shear stress in nominally two-dimensional boundary layers which they attribute to non-uniformities generated by the last screen in the settling chamber. A theoretical analysis of Crow (1966) has shown, that small non-uniformities of the approach flow produce considerable variations in laminar boundary layers.

It was suggested by Bohl (1940) and reviewed by Morgan (1960) that the flow behind screens may, under certain conditions, be unstable and small irregularities of the screen may cause the coalescence of groups of jets. For sufficiently large open area ratios the regular pattern of jets is found to be stable. Bradshaw (1965), therefore, recommends using screens with an open area ratio (open area/total area) of $\beta > 0.57$. Mehta (1985) points to the effect of weaving properties: woven metal screens produce more non-uniformities than flat plastic screens and a correlation with the uniformity of weave is found.

Non-uniformities of the flow, as brought about by screens and grids, have also been quoted as the probable cause for the regular pattern of longitudinal vortices that is often observed in the stagnation region of cylindrical bodies placed normal to the main flow direction. A review and detailed discussion of the phenomenon in question

is given by Morkovin (1979). Flow instability as well as the direct effect of non-uniformities of the oncoming flow have been considered as possible causes for the observed vortex pattern.

The possibility that the flow near the stagnation point may become unstable was first suggested by Görtler (1955) who pointed out that the streamlines near the stagnation point have a concave curvature, and the flow in the boundary layer may, therefore, be subject to a centrifugal instability analogous to the flow over concave surfaces. The very regular pattern of longitudinal vortices observed e.g. by Colac-Antik (1971) apparently supports the instability hypothesis. A mathematical treatment of the stability problem by Hämmerlin (1955) led him to the conclusion that the stagnation-point flow is unstable. It was felt, however, that the results of Hämmerlin are unsatisfactory and the problem was re-examined by Kestin & Wood (1970) and again by Wilson & Gladwell (1978), who concluded, as Hainzl (1965) had, that the stagnation-point flow is stable.

Another approach to explain the occurrence of longitudinal vortices in the stagnation flow is the 'vorticity amplification theory' of Sutera, Maeder & Kestin (1963) and Sutera (1965). It is assumed that finite disturbances are generated in the approaching flow, e.g. by screens or grids in the settling chamber of the wind tunnel. In general, the disturbances contain vorticity with components in all spatial directions. Following the streamlines past the stagnation point, the flow is accelerated and the vorticity component parallel to the local flow direction is stretched. The stretching of the vorticity increases the vortical velocity and leads to the observed vortical structures. Sadeh, Sutera & Maeder (1970*a*) extended the boundary-layer theory of vorticity amplification into the outer flowfield. In an experimental study, Sadeh *et al.* (1970*b*) verified that the rate of amplification depends on the scale of the disturbances in accordance with the theoretical predictions. Hodson & Nagib (1975) have shown experimentally that the wake downstream of a single wire produces a counter-rotating vortex pair in the stagnation region (see figure 8) in accordance with the theory of Sutera (1965).

Our experimental results support the view of Sutera (1965) that finite disturbances of the approach flow are responsible for the observed pattern of longitudinal vortices in the stagnation region of cylindrical bodies, whereas no indication of flow instability was found. Assuming that the observed flow pattern is merely the result of non-uniformities of the approach flow it appears difficult, however, to explain why rather regular, almost periodical structures are observed and which mechanism determines the wavelength of the periodical structures.

In order to get more insight into the phenomenon, the flowfield downstream of screens and grids was thoroughly investigated by flow-visualization experiments. Section 2 gives a description of the experimental apparatus and procedures. In §3 the experimental results concerning the flow downstream of screens and grids are presented and in §4 the influence of screens on the stagnation flow of circular cylinders is discussed. Finally, in §5 an attempt is made to explain the experimental results by means of a simplified model of the flow through grids.

## 2. Experimental apparatus and procedures

In order to investigate the non-uniformities of the flow generated by screens and grids it was considered essential that the upstream conditions of the test flow are as uniform as possible. For this reason the experiments were carried out in a water tow

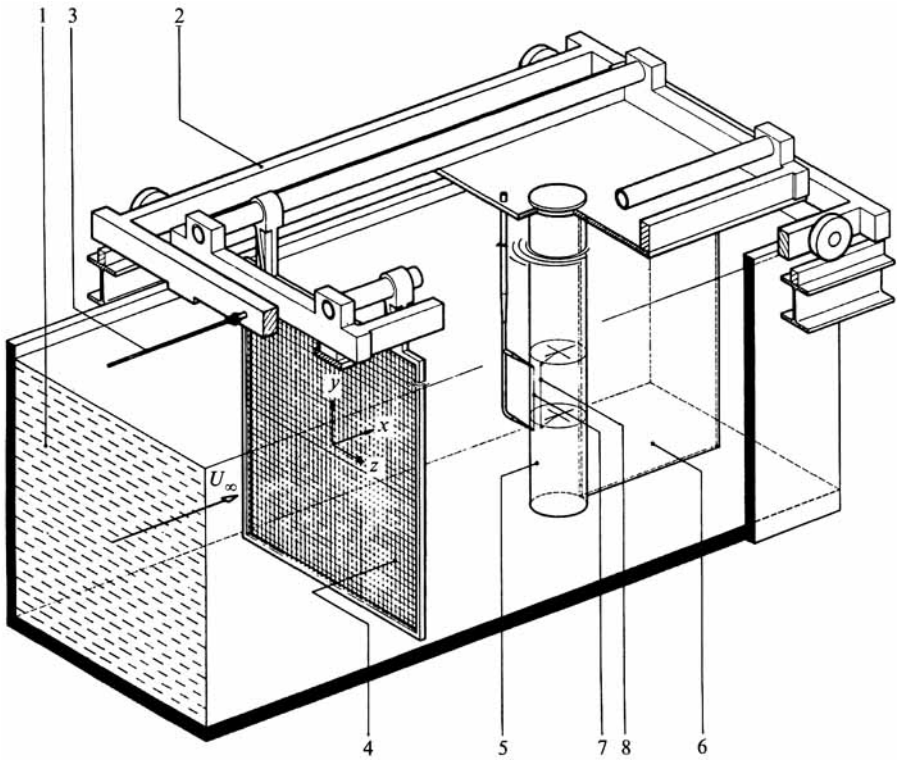


FIGURE 1. Experimental set-up in the water towing tank of the DFVLR. 1, water tank; 2, towing carriage; 3, towing rope; 4, screen; 5, circular cylinder; 6, splitter plate; 7, hydrogen-bubble probe 1; 8, hydrogen-bubble probe 2.

tank where the upstream conditions can be controlled more readily than in a closed water tunnel or wind tunnel.

The water tow tank of the DFVLR Göttingen is 18 m long and has a cross-section of 1.1 m × 1.1 m. A detailed description of the tank was given by Bippes (1972). Figure 1 shows a typical experimental set-up. The flow was investigated by towing the model (a screen or a screen with cylinder mounted downstream) through the water at rest. For flow visualization the hydrogen-bubble technique was used. The figure shows the arrangement of two hydrogen-bubble probes. A coordinate system is used with the $x$-axis oriented in the mean flow direction and the origin $x = 0$ at the screen plane. The $y$-axis is aligned with the cylinder axis and the $z$-axis is normal to the $x$ and $y$-axis (figure 1).

The flowfield downstream of eight woven screens with different geometries was investigated. The open area ratio of the screens was in the range $0.45 \leqslant \beta \leqslant 0.75$. In addition, grids of parallel rods and one flat screen were used. In this paper the results from three screens and two grids with different geometries are discussed. These screens and grids were investigated most extensively and lead to the main conclusions. The dimensions of the screens are shown in table 1. For further results see Böttcher (1987).

The free-stream velocity, i.e. the tow velocity, was varied in the range $0.03\,\mathrm{m/s} < U_\infty < 0.8\,\mathrm{m/s}$, corresponding to Reynolds numbers of $9 < Re_d < 240$ where $Re_d = U_\infty d/\nu$ with $d$ as the wire diameter and $\nu$ the kinematic viscosity of water. By

| Screen/grid no. | $d$ (mm) | $M$ (mm) | $\beta = (1-d/M)^2$ |
|---|---|---|---|
| Screen no. 6 | 0.30 | 1.10 | 0.53 |
| Screen no. 7 | 0.30 | 1.23 | 0.57 |
| Screen no. 8 | 0.30 | 2.28 | 0.75 |
| Grid no. 1 | 0.30 | 2.00 | 0.85 |
| Grid no. 2 | 0.30 | 4.00 | 0.93 |

TABLE 1. Dimensions of screens and grids

using two cylinders with different diameters $D = 80$ mm and 200 mm the model Reynolds number $Re_D = U_\infty D/\nu$ could be varied in the range $2400 < Re_D < 160000$. The distance $x$ between screen and hydrogen bubble probe or stagnation point of the cylinder, respectively, was varied in the range 5 mm $< x <$ 1460 mm.

## 3. The flow downstream of screens and grids

Figure 2 shows typical time line photographs of the flow downstream of a screen. The flow direction is from left to right. The hydrogen bubble wire is placed at a distance $x$ downstream of the screen. Time lines are generated by a pulsating voltage on the wire. Since the wire is pulsed periodically, a set of equally spaced time lines appears downstream of the wire. The spacing is $\Delta x = U\Delta t = 11$ mm, where $\Delta t$ is the time interval between two consecutive pulses and $U$ the stream velocity. The time lines closest to the hydrogen-bubble wire are shaped as the local velocity profile (i.e. the velocity profile at the location of the wire). The shape of the time lines further downstream has not a simple interpretation – it is determined by the infinite set of velocity profiles the time line has experienced between its birth and the time of observation. If the velocity profiles are not changing much between the hydrogen-bubble wire and the locus of observation, the shape of the time line approximates a mean velocity profile.

At large distances behind the screen the spanwise variations of the velocity become very small, i.e. the velocity profile is nearly uniform (figures 2*c* and 2*d*). The small velocity variations appear enlarged when the time lines are observed at a larger distance from the wire. For this reason, a large number of time lines is displayed in each of the figures.

Immediately behind the screen (figure 2*a*) a periodic pattern of jets and wakes is formed that reflects the structure of the screen, i.e. the spacing of the wakes is equal to the mesh size. Further downstream the jets and wakes appear to coalesce to the effect that the number of jets and wakes is reduced (figure 2*b*). At $x = 570$ mm (figure 2*c*) the distance between adjacent jets – briefly denoted as 'wavelength' – has increased further. At still larger distances, $x \geqslant 1400$ (figure 2*d*), the wavelength remains constant. Figure 3(*a*–*c*) shows the wave pattern of three different screens in comparison.

A large number of hydrogen-bubble pictures was evaluated to determine the evolution of the wavelength $\lambda$. In figure 4(*a*–*c*) the averaged wavelength, normalized with the mesh size $M$, is plotted versus the distance $x$ for screens nos. 6, 7 and 8. Here the averaged wavelength is the length of the hydrogen-bubble wire divided by the number of waves. Every peak that could be resolved was counted as one wave. A comparison of figures 4*a*, 4*b* and 4*c* shows that similar results are obtained for the

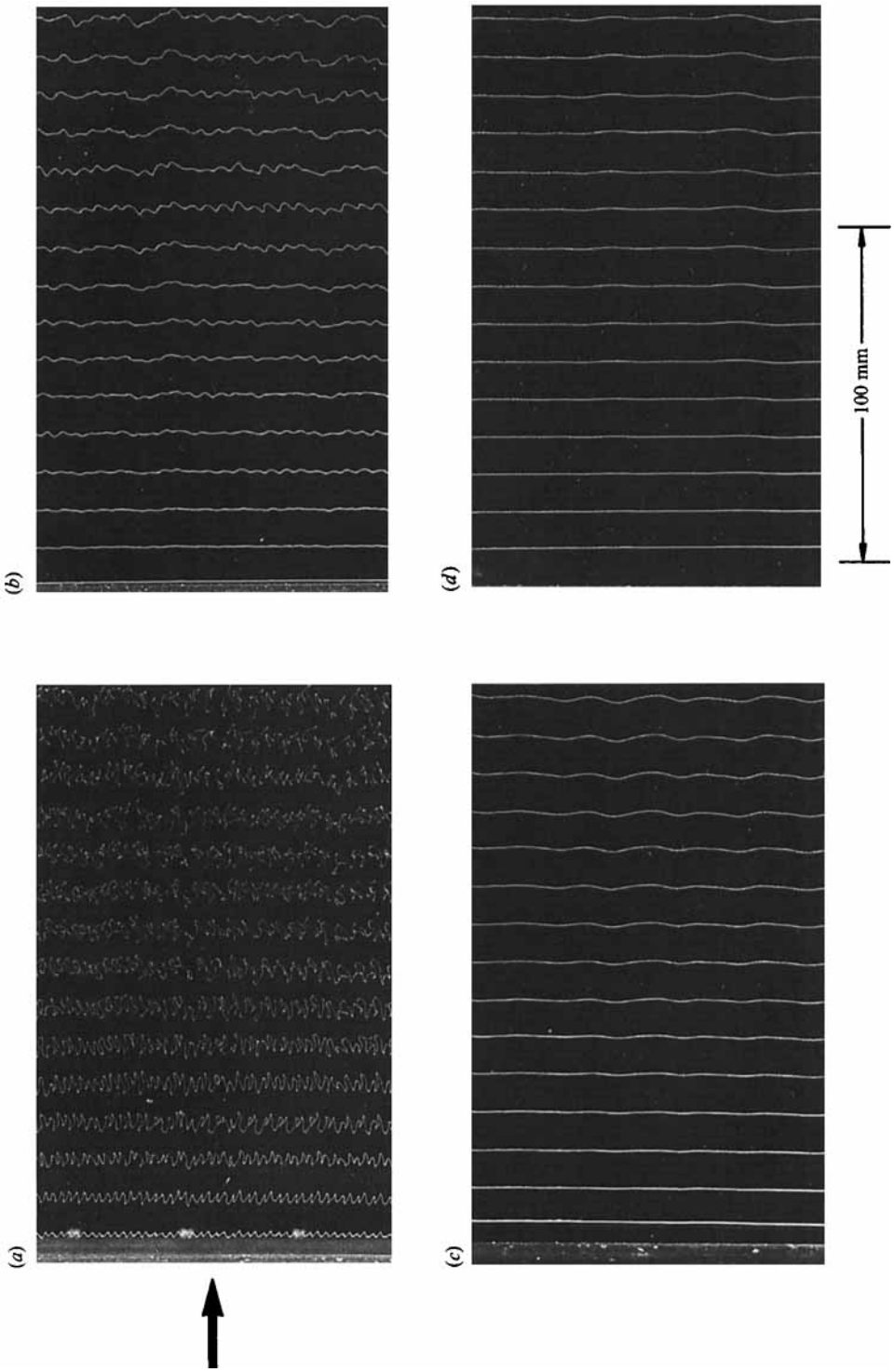


FIGURE 2. The flow downstream of screen no. 8 for different distances $x$ from the screen. Flow from the left. $U_\infty = 0.16$ m/s, $Re_d = 48$. (*a*) $x = 20$ mm; (*b*) $x = 90$ mm; (*c*) $x = 570$ mm; (*d*) $x = 1400$ mm.

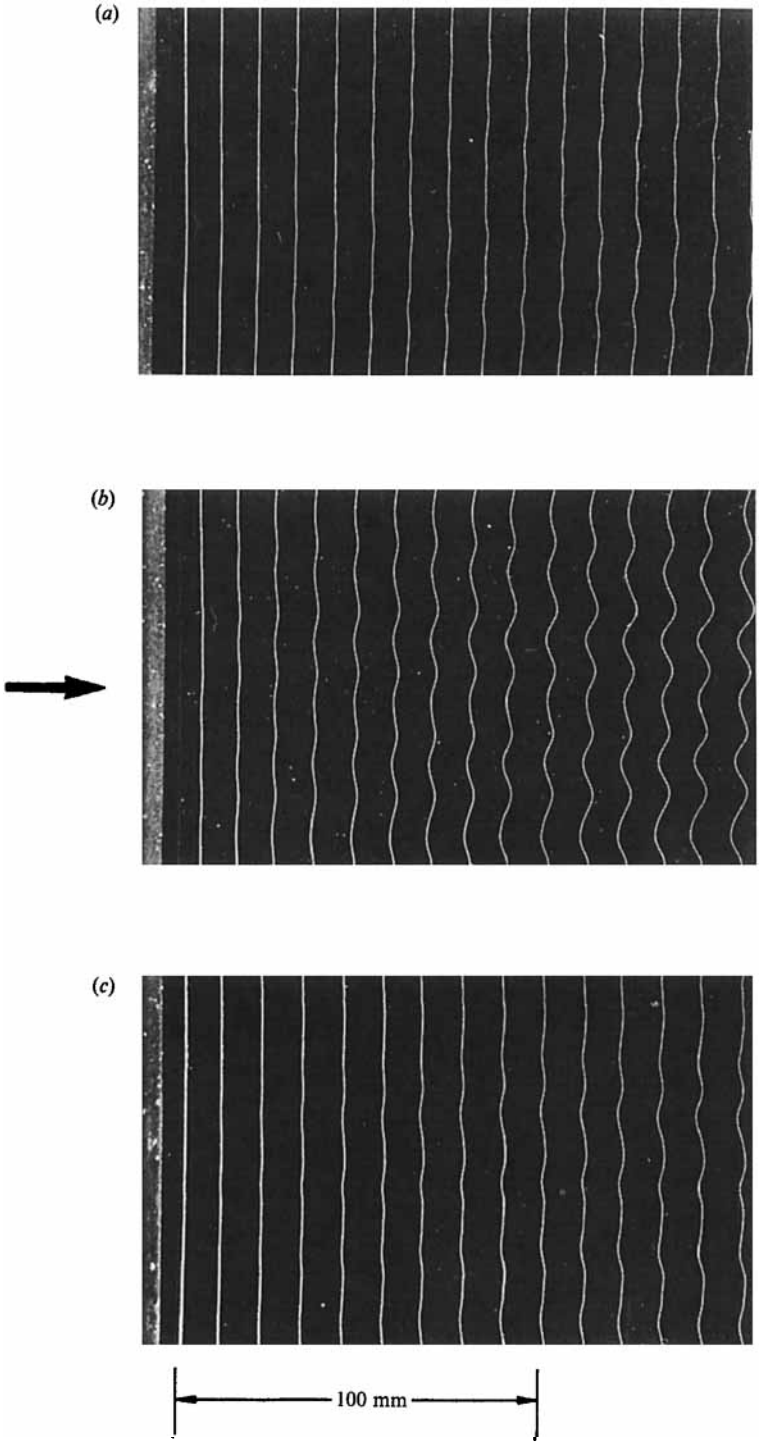


FIGURE 3. The flow downstream of (*a*) screen no. 6, $\beta = 0.53$; (*b*) screen no. 7, $\beta = 0.57$; (*c*) screen no. 8, $\beta = 0.75$. $x = 570$ mm, $U_\infty = 0.16$ m/s, $Re_d = 48$.

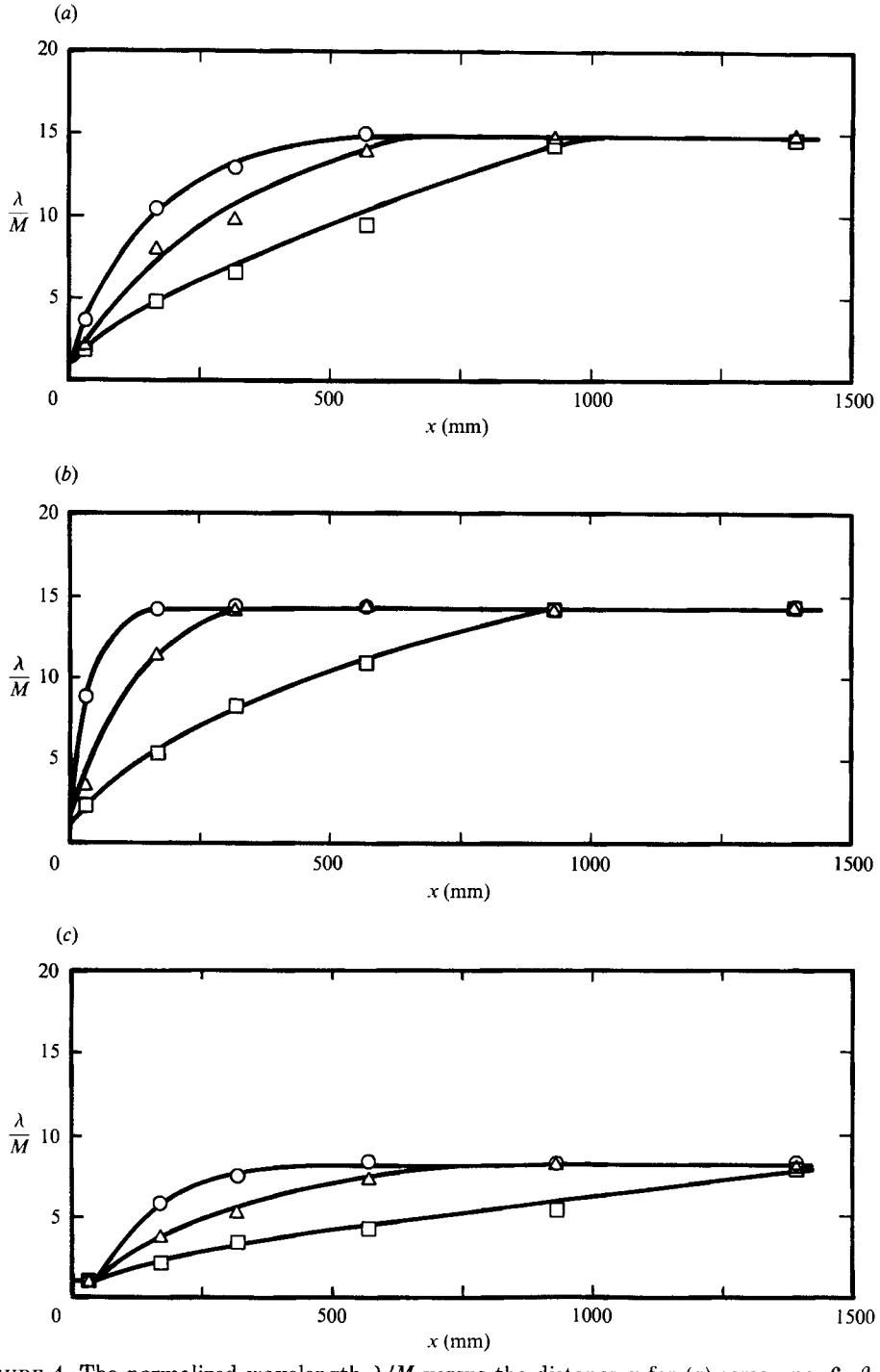


FIGURE 4. The normalized wavelength $\lambda/M$ versus the distance $x$ for (*a*) screen no. 6, $\beta = 0.53$; (*b*) screen no. 7, $\beta = 0.57$; (*c*) screen no. 8, $\beta = 0.75$. ○, $U_\infty = 0.10$ m/s; △, $U_\infty = 0.16$ m/s; □, $U_\infty = 0.37$ m/s.

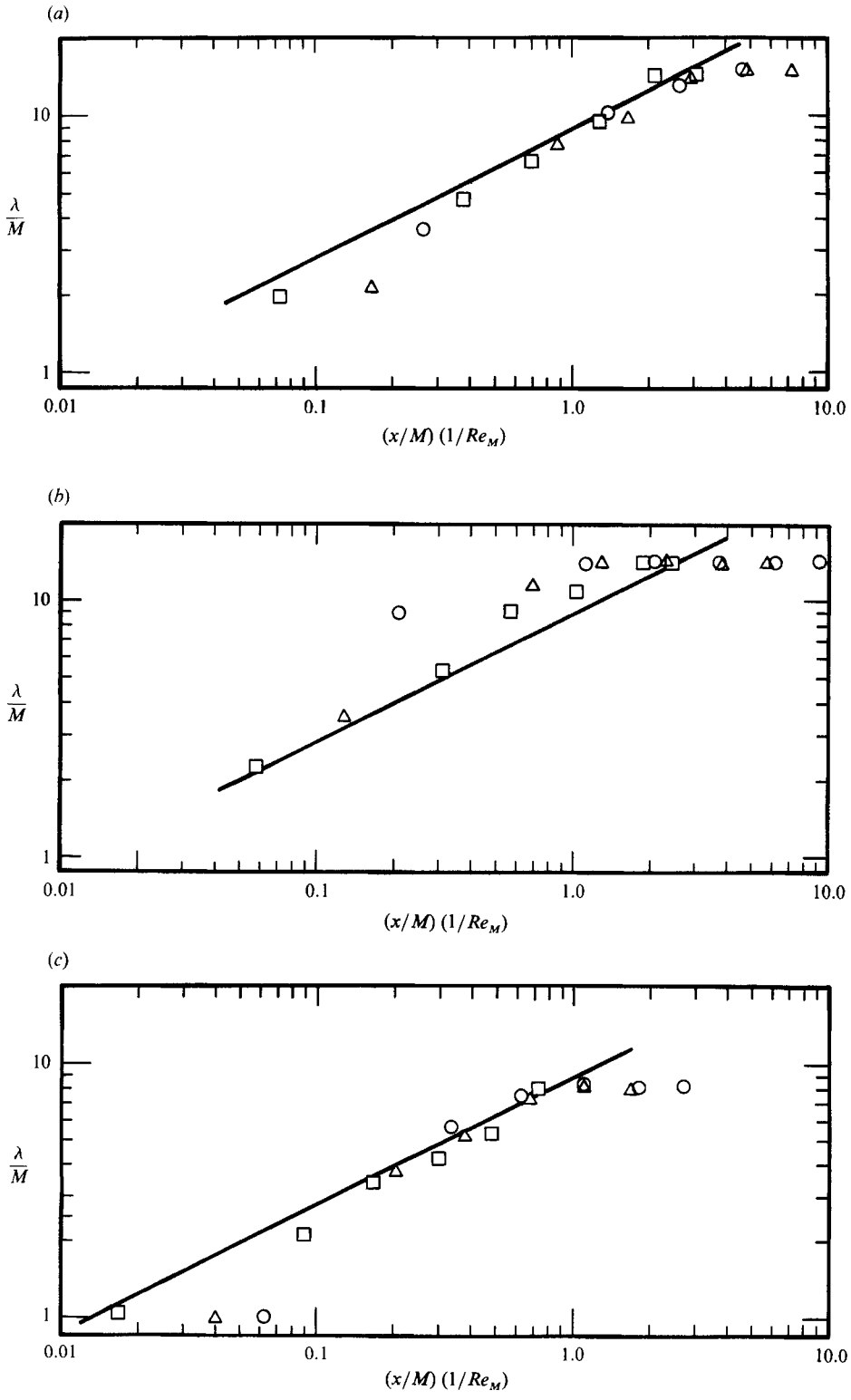


FIGURE 5. The normalized wavelength $\lambda/M$ versus $(x/M)(1/Re_M)$ in logarithmic scale for screens nos. 6, 7 and 8. Details as for figure 4. ——, theory.

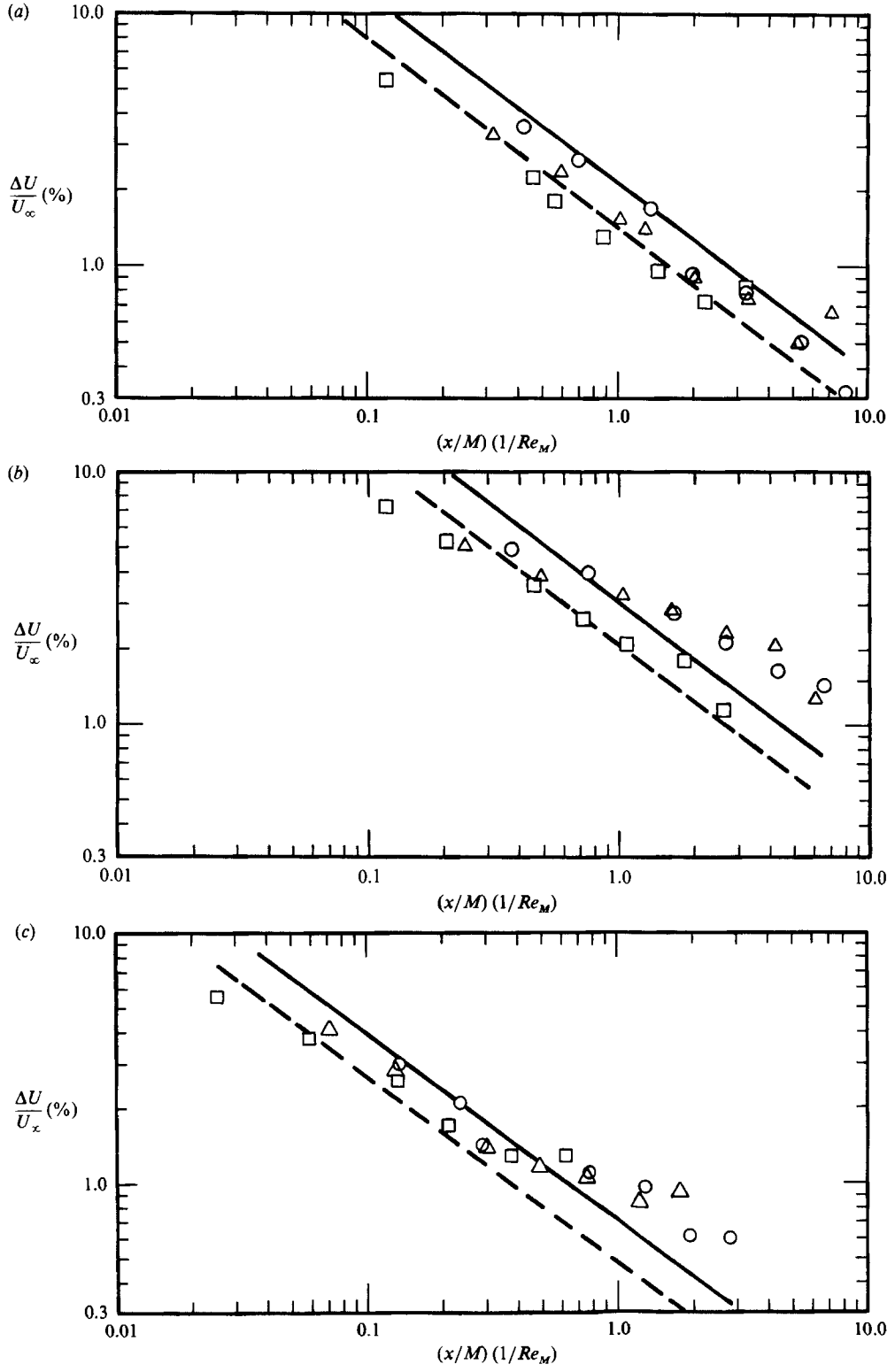


FIGURE 6. The velocity variation $\Delta U/U_\infty$ versus $(x/M)\,(1/Re_M)$ for the screens nos. 6, 7 and 8 in logarithmic scale. ——, theory for $U_\infty = 0.10$ m/s. – – –, theory for $U_\infty = 0.37$ m/s. Standard deviation: (*a*) $\sigma = 0.035$; (*b*) $\sigma = 0.065$; (*c*) $\sigma = 0.045$. Other details as for figure 4.

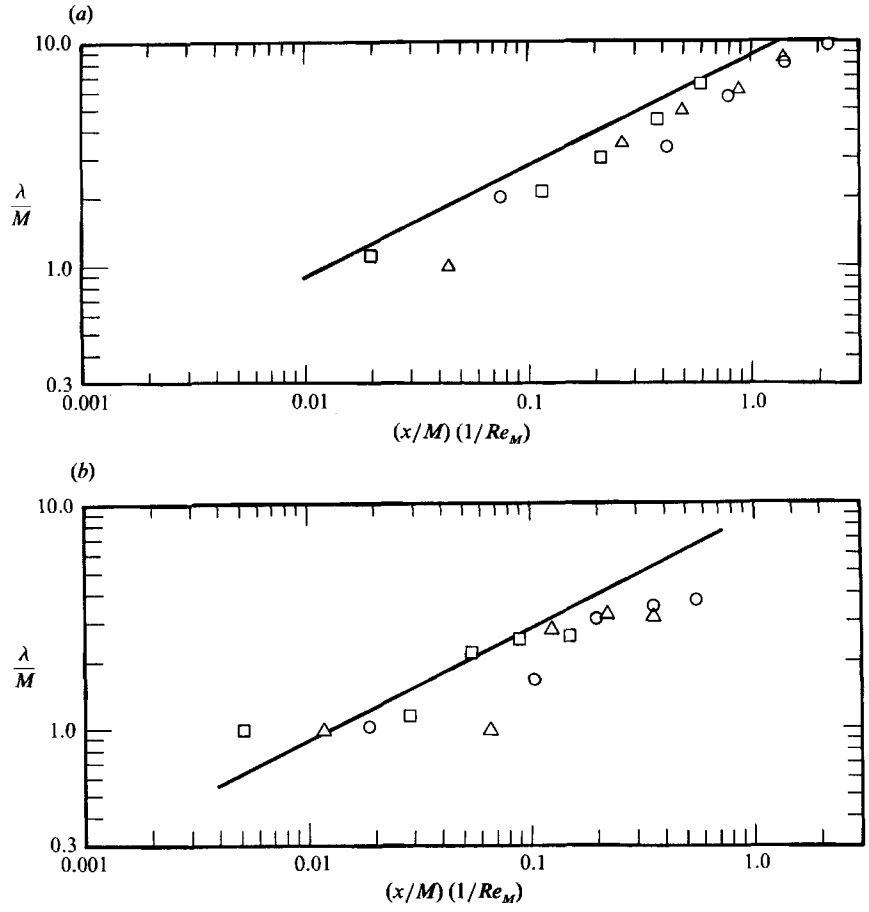


FIGURE 7. The normalized wavelength $\lambda/M$ versus $(x/M)(1/Re_M)$ for (*a*) grid no. 1 and (*b*) no. 2 in logarithmic scale. —— theory. ○, $U_\infty = 0.10$ m/s; △, $U_\infty = 0.16$ m/s; □, $U_\infty = 0.37$ m/s.

different screens. Close to the screens $\lambda/M = 1$ as may be expected. Further downstream the wavelength increases until a final value is reached. The increase of $\lambda/M$ is dependent on the free-stream velocity $U_\infty$. The final wavelength depends on the screen geometry.

Plotting $\lambda/M$ versus a normalized distance $\bar{x} = x/(MRe_M)$ (figure 5*a–c*) the curves for different free-stream velocities $U_\infty$ collapse onto one curve. The solid lines in figure 5(*a–c*) show the result of a theoretical analysis presented in §5.

Naturally, the disturbances generated by a screen decrease with increasing distance from the screen. The decrease is apparent from the photographs of figure 2(*a–d*) which show the reduction of the amplitude with increasing $x$. The amplitude reduction is discussed in more detail because this quantity can be compared with theoretical predictions.

In figure 6(*a–c*) the normalized velocity variation $\Delta U/U_\infty$ is plotted versus the normalized distance $\bar{x} = x/(MRe_M)$ for the three screens. Here the velocity variation is defined as $\Delta U = U_{\max} - U_{\min}$, where $U_{\max}$ and $U_{\min}$ are the observed maximum and minimum velocities, which have been determined by evaluation of the hydrogen-bubble photographs. The figure shows that a plot of $\Delta U/U_\infty$ versus $x/(MRe_M)$ gives a straight line in double logarithmic scale which is almost independent of $U_\infty$. The

theoretical results, which are discussed in §5 are also plotted in figure 6(*a–c*) as solid or broken lines. Apparently, the theoretical approach describes the experimental results quite well.

Additional tests have been performed on grids of parallel rods. The investigation of the flow downstream of grids is of particular interest because screens can be regarded as composed of two grids positioned perpendicular to each other.

In all cases reported here the grid wires were perpendicular to the observation plane. The wire diameter was 0.3 mm and the mesh size (spacing of the wires) was 2 mm and 4 mm respectively (see table 1). Details of the construction of the grids are described by Böttcher (1987).

Results of a systematic evaluation of a large number of hydrogen-bubble pictures are shown in figure 7(*a–b*). As in figure 5(*a–c*) for the screens the normalized wavelength is plotted versus the normalized distance $x/(MRe_M)$ with the effect that all the data for different $U_\infty$ collapse onto one curve. As for the screens (figure 5*a–c*), the normalized wavelength increases with $x/(MRe_M)$. In figure 7(*a–b*) also the theoretical result is plotted as a solid line. The theoretical curve has about the correct slope but is somewhat higher than the experimental points.

## 4. The influence of screens on the flow in the stagnation region of cylinders

Hodson & Nagib (1975) have shown that the wake of a single wire generates a vortex pair in the stagnation region of a cylinder downstream from the wire (see figure 8). The reversed flow between the counter-rotating vortices is caused by the pressure rise near the stagnation point. To investigate the influence of a screen on the stagnation flow, a circular cylinder was mounted downstream of the screen. Figure 9 shows a typical photograph of the flow in the stagnation region. Every hydrogen-bubble line on the cylinder represents a pair of counter-rotating vortices (see Colak-Antic 1971). The experimental parameters were chosen so that the final wavelength was reached. Compared with the experiment of Hodson & Nagib (1975), using a single wire, the flow downstream of the screen is more complex. Nevertheless, figure 9 shows that essentially the same phenomenon occurs in the stagnation region. For each wake a pair of counter-rotating vortices develops. We therefore denote the distance between two adjacent vortex pairs also as wavelength.

With no screens upstream of the cylinder no longitudinal vortices in the stagnation region could be observed, not even for large model Reynolds numbers of up to $Re_D = 700\,000$. Figure 10 shows photographs for various distances $x$ between screen and cylinder. The photographs correspond to those shown in figure 2 except that now the cylinder is present. For a very small distance $x$ (figure 10*a*) a vortex pair develops for every mesh. In figure 10*b* the number of vortex pairs is reduced. In figure 10*c*, for a distance $x = 600$ mm, the final wavelength is reached. In figure 10*d* the number of vortex pairs has not changed compared with figure 10*c*, but the vortex strength is reduced because the amplitude of the oncoming disturbance decreases continually downstream.

Figure 11 shows the flow in the stagnation region for a case where the disturbances were generated by a grid of parallel rods. The photograph clearly shows the evolution to increasingly larger wavelengths.

In figure 12 the results of a systematic evaluation for the screens nos. 6, 7 and 8 and a cylinder diameter $D = 80$ mm are plotted. The final wavelength is neither dependent on the diameter of the cylinder nor on the existence of a cylinder at all

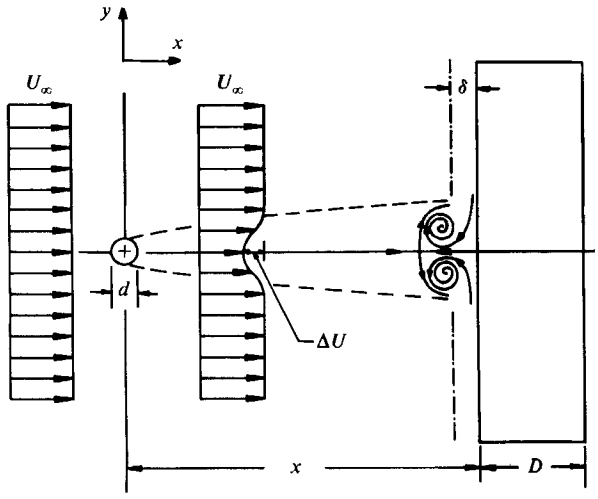


FIGURE 8. Development of a counter-rotating vortex pair in the stagnation region (Hodson & Nagib 1975).

(compare figure 12 with figure 4). The relation between the wavelength and the distance behind the screen is slightly changed owing to the deceleration of the flow in the stagnation region.

The results of the experiments with screens plus cylinder demonstrate that the vortical flow observed in the stagnation region of the cylinder is not initiated by the cylinder, but the cylinder is merely an indicator of the flow pattern that already exists in the approach flow and which is amplified in the stagnation region. With no disturbances in the oncoming flow, no longitudinal vortices develop in the stagnation region. The present investigation gives no indication for the existence of an instability as proposed by Görtler (1955).

To confirm the last statement, additional experiments were carried out in a water tunnel. At a distance $x = 500$ mm upstream of a circular cylinder (with diameter $D = 80$ mm) a wire ($d = 2$ mm) was suddenly brought into the flow and the time interval $\Delta t_1$, was measured which elapsed until a longitudinal vortex pair appeared in the stagnation region of the cylinder. Again the hydrogen-bubble technique was used for flow visualization. In a second experiment the wire was withdrawn suddenly and the time interval $\Delta t_2$ was measured, until the pair of longitudinal vortices disappeared. The measurements were performed at free-stream velocities $U_\infty = 0.05$ m/s, 0.10 m/s and 0.23 m/s corresponding to Reynolds numbers of $Re_D = 4000$, 8000 and 18400. In figure 13, $\Delta t_1$ and $\Delta t_2$ are plotted versus $Re_D$. Apparently it is $\Delta t_1 = \Delta t_2$ within the accuracy of the measurements. The fact that the pair of longitudinal vortices appears and again disappears after exactly the time it takes to convect the upstream disturbance towards the cylinder proves that the observed vortical patterns are a direct result of the non-uniformity of the flow and that the stagnation flow is stable with respect to small disturbances within the experimental range of Reynolds numbers.

## 5. Theoretical analysis of the flow behind grids

In this section an attempt is made to explain the experimental results of the previous sections, namely the fact that fairly regular velocity variations are observed

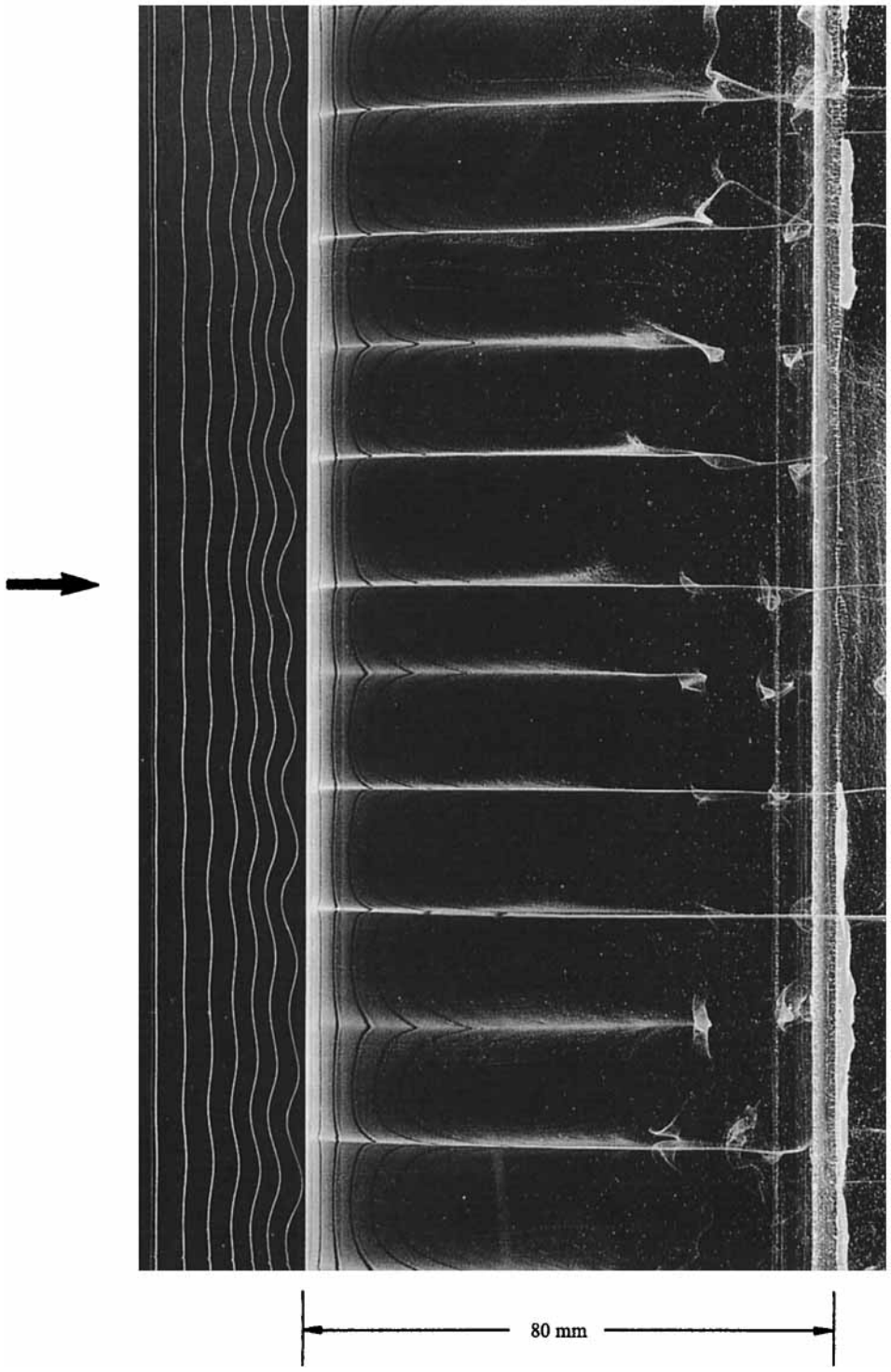


FIGURE 9. The flow in the stagnation region of a circular cylinder. The disturbances were generated by screen no. 7. Flow from the left. $U_\infty = 0.16$ m/s, $Re_d = 48$, $x = 930$ mm, $D = 80$ mm.

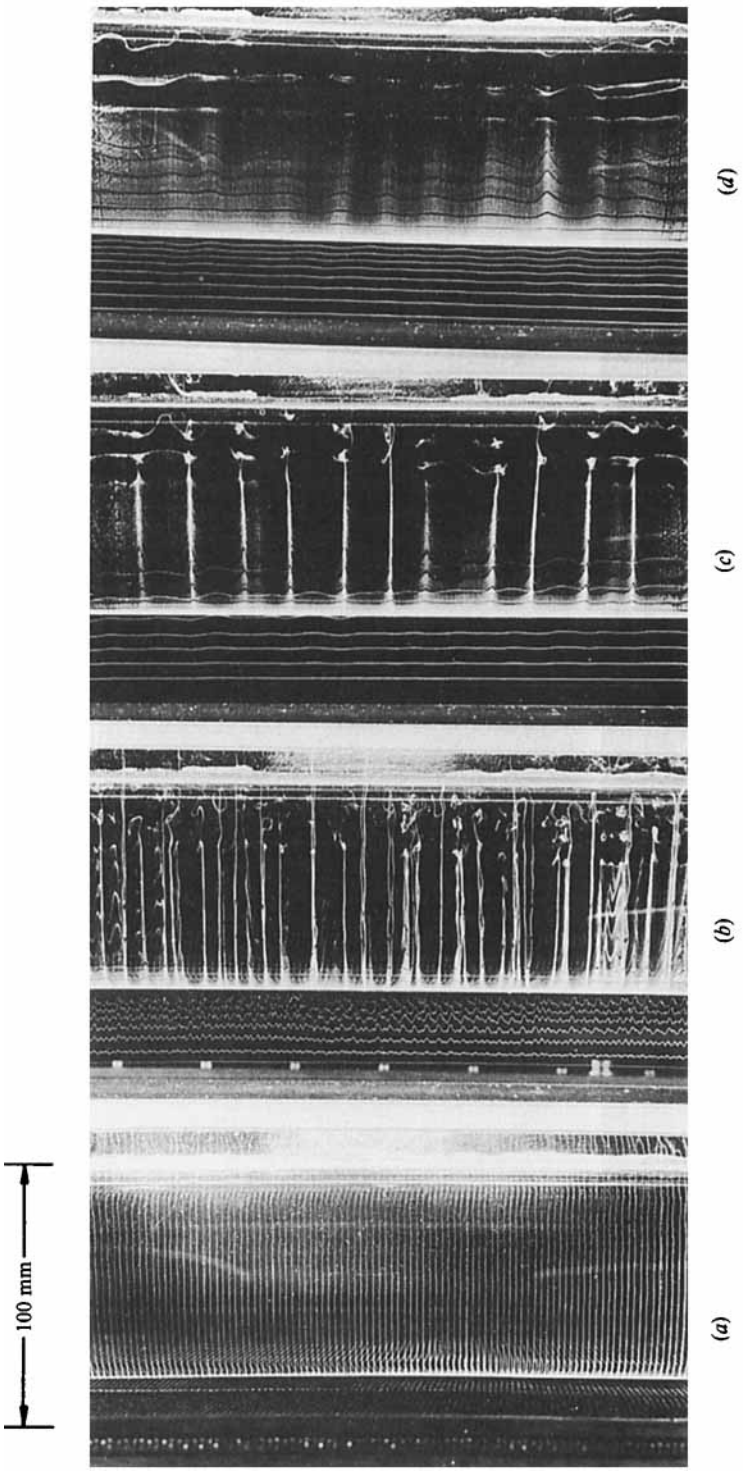


FIGURE 10. The flow in the stagnation region of a circular cylinder for different distances from screen no. 8. Flow from the left. $U_\infty = 0.16$ m/s, $Re_d = 48$, $D = 80$ mm. (*a*) $x = 5$ mm; (*b*) $x = 60$ mm; (*c*) $x = 600$ mm; (*d*) $x = 1460$ mm.

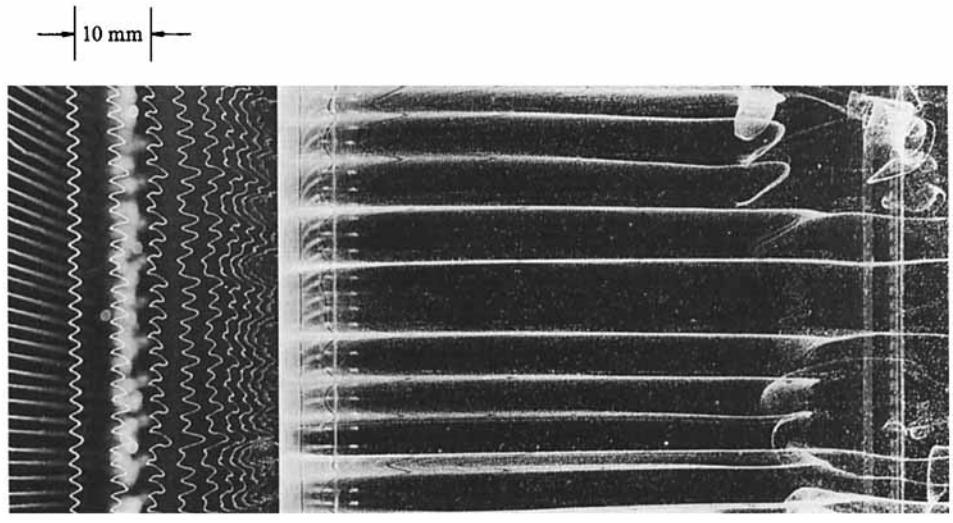


FIGURE 11. The flow in the stagnation region of a circular cylinder. The disturbances were generated by an array of parallel rods. Flow from the left. $M = 2.0$ mm, $d = 0.3$ mm, $U_\infty = 0.10$ m/s, $Re_d = 30$, $x = 40$ mm, $D = 80$ mm.

in the wake of screens and grids and that the wavelength of the variations is continually increasing in the downstream direction until the amplitude of the disturbances is decreased below a small percentage of the free-stream velocity.

The theory presented in the following does not assume, as is usually done, that the velocity variations are brought about by the coalescence of two or more jets emerging from the screen pores although it shall not be questioned that the coalescence of jets, or wakes, may be observed under certain conditions. The theoretical analyses of Bohl (1940) indicate that coalescence of jets may occur as the result of flow instability provided that the intensity of the jets is large, i.e. the variation of the velocity between jets and wakes is not small compared with the mean velocity. Observations have shown, however, that the wavelength of the disturbances increases downstream even though the amplitude becomes extremely small.

An obvious explanation for the increase of wavelength in the downstream direction is that the small wavelength components are more rapidly damped than disturbances of larger wavelengths. It will be assumed in the following that woven screens are not perfectly uniform, i.e. the mesh size is not exactly constant but varies in a random way. As a result, the wake behind the screen not only contains variations having a wavelength equal to the mesh size and its harmonics, but also variations with larger wavelengths. In fact, velocity disturbances with a continuous spectrum of wavenumbers will be generated by the random variations of the mesh size. Why then are the variations downstream of the screen fairly regular, showing a dominant wavelength? The answer is roughly as follows. The spectrum of wavelengths is cut off at very small wavelengths because these are rapidly damped. The very large wavelengths are cut off because the generation of large wavelength components (by random variations of mesh size) is very improbable as will be shown by the following analysis.

There remains a fairly small band of wavelengths of those spectral components that are sufficiently large to be observable downstream of the screen.

Since the wake behind a screen can, approximately, be made up of the wakes of

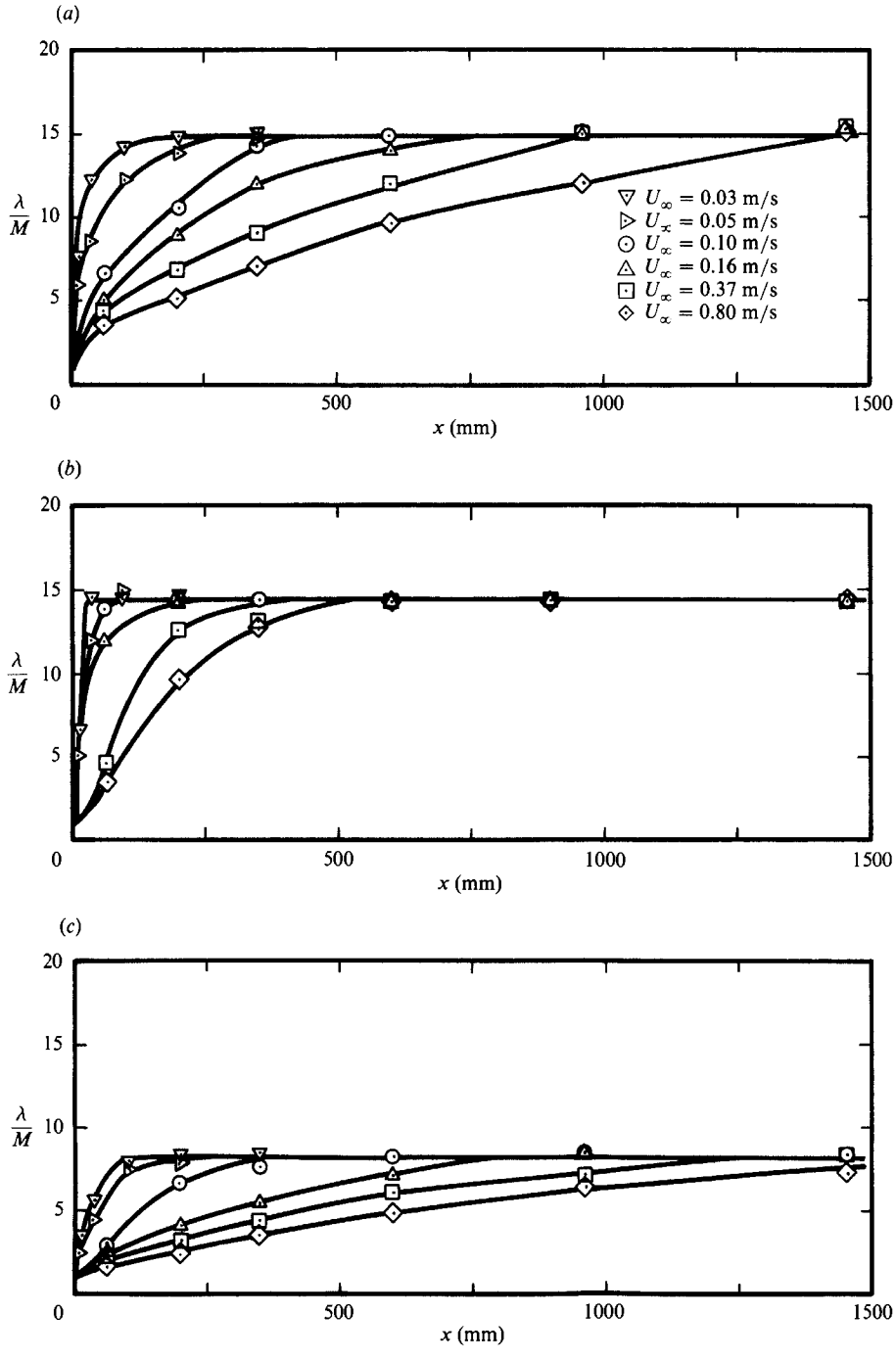


FIGURE 12. The normalized wavelength $\lambda/M$ versus the distance $x$ between screen and stagnation point of a circular cylinder (diameter $D = 80$ mm). (*a*) screen no. 6, $\beta = 0.53$; (*b*) screen no. 7, $\beta = 0.57$; (*c*) screen no. 8, $\beta = 0.75$.

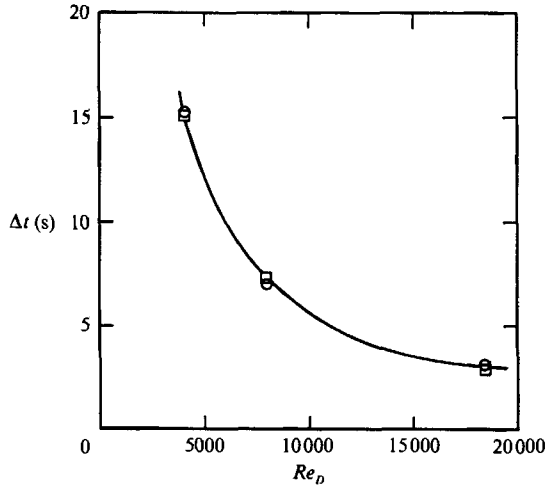


FIGURE 13. Time lag versus Reynolds number $Re_D$. ○, $\Delta t_1$: time lag of the appearance of a vortex pair. □, $\Delta t_2$: time lag of the disappearance of a vortex pair.

two grids, oriented at 90° to each other, the following analysis can be restricted to a two-dimensional wake behind a grid of parallel rods.

The velocity distribution behind a grid of $N$ parallel rods at positions $y_n$ is:

$$u = U - \sum_{n=1}^{N} W(y-y_n) = U-u', \tag{1}$$

where $U$ = constant and the 'wake function' $W(y-y_n)$ describes the velocity-defect profile behind a single rod at position $y_n$.

In order to calculate the velocity distribution at a large distance downstream of the grid, we consider the Fourier decomposition of $u'$:

$$u' = \sum_{n=1}^{N} W(y-y_n) = \sum_{K=-\infty}^{\infty} a_K \exp\left(\frac{2\pi i K y}{l}\right), \tag{2}$$

where $l$ is the width of the grid, which is the number of rods $N$ times the average spacing $M$, i.e.

$$l = MN. \tag{3}$$

According to (2) the wake is assumed to be periodic with period $l = NM$. This assumption is not a serious restriction if $N$ is a sufficiently large number.

Assuming that $u' \ll U$, the equation of motion for $u'$ is, in linear approximation:

$$U\frac{\partial u'}{\partial x} = \nu\frac{\partial^2 u'}{\partial y^2}. \tag{4}$$

The initial distribution of $u'$ (at $x = 0$) is given by (2). With this initial condition the solution of (4) is:

$$u' = \sum_{K=-\infty}^{\infty} a_K \exp\left(\frac{2\pi i K y}{l}\right)\exp\left(\frac{-4\pi^2 K^2 \nu x}{Ul^2}\right). \tag{5}$$

The coefficients $a_K$ follow from Fourier transformation of (2):

$$a_K = \frac{1}{l}\int_0^l \sum_{n=1}^{N} W(y-y_n)\exp\left(\frac{-2\pi i K y}{l}\right)\mathrm{d}y. \tag{6}$$

We are mainly concerned with the Fourier components for small wavenumbers $-N < K < N$ (i.e. large wavelength $\lambda > M$) since these are the only ones that survive far downstream from the grid, while the large wavenumber components decrease rapidly with increasing $x$ as shown by the exponential factors $\exp(-4\pi^2K^2\nu x/Ul^2)$ in (5).

Now, for small wavenumbers ($-N < K < N$) the width of the wake function $W(y-y_n)$ is small compared with the wavelength $\lambda > M$ so that the wave factors $\exp(-2\pi iKy/NM)$ in (6) do not change appreciably over the width of the function $W(y-y_n)$, which therefore acts like a Dirac $\delta$-function on the wave factors and (6) can be approximated by:

$$a_K = \frac{q}{l}\sum_{n=1}^{N}\exp\left(\frac{-2\pi iKy_n}{l}\right), \tag{7}$$

with

$$q = \int_{\text{wake}} W(y)\,\mathrm{d}y. \tag{8}$$

For a perfect grid the rods are at positions $y_n = Mn$ and, according to (7) the coefficients $a_K$ are zero except for $K = 0, N, 2N, 3N, \ldots$, reflecting the fact that the wake is periodic, like the grid, with period $M$.

Large wavelength components of the wake flow are generated by irregularities of the grid. To investigate the effect of irregularities, we assume that:

$$y_n = M(n+\delta_n), \tag{9}$$

where the $\delta_n$ are small random numbers, $|\delta_n| \ll 1$. The average value of $\delta_n$ is zero and the standard deviation (variance) is

$$\sigma^2 = \overline{\delta_n^2}. \tag{10}$$

Inserting (9) into (7) gives, with $l = MN$:

$$a_K = \frac{q}{MN}\sum_{n=1}^{N}\exp\left(\frac{-2\pi iKn}{N}\right)\exp\left(\frac{-2\pi iK\delta_n}{N}\right). \tag{11}$$

For $|K| < N$ and $|\delta_n| \ll 1$ the second factors in (11) can be approximated by:

$$\exp\left(\frac{-2\pi iK\delta_n}{N}\right) \approx 1 - \frac{2\pi iK\delta_n}{N}$$

and (11) becomes:

$$a_K = \frac{q}{NM}\sum_{n=1}^{N}\exp\left(\frac{-2\pi iKn}{N}\right) - \frac{q}{NM}\frac{2\pi K}{N}\sum_{n=1}^{N} i\delta_n \exp\left(\frac{-2\pi iKn}{N}\right). \tag{12}$$

The first sum in (12) represents the Fourier components for a perfect grid, which are different from zero only for $|K| = 0, N, 2N, \ldots$. The component with $K = 0$ corresponds to a constant mean velocity of the wake while the large wavenumber components with $K = N, 2N, 3N, \ldots$, are rapidly damped in the downstream direction. We therefore retain only the second term of (12) which represents the Fourier components with small wavenumbers $0 < |K| < N$. Writing

$$\Delta_K = \sum_{n=1}^{N} -i\delta_n \exp\left(-\frac{2\pi iKn}{N}\right), \tag{13}$$

it can be shown at once, that the quantities $\Delta_K$ are again (complex) random numbers having zero mean values and the variance:

$$\overline{|\Delta_K|^2} = N\overline{\delta_n^2} = N\sigma^2. \tag{14}$$

Thus we have: $$a_K = \frac{q}{NM}\frac{2\pi K}{N}\Delta_K \quad \text{for } 0 < |K| < N. \tag{15}$$

Inserting (15) into (5) and interpreting (5) only for large values of $x$, so that the Fourier components with $|K| \geqslant N$ can be neglected, we obtain

$$u' = \frac{2\pi q}{NM}\sum_{K=-\infty}^{\infty}\frac{K}{N}\Delta_K \exp\left(\frac{2\pi i K y}{NM}\right)\exp\left(-\frac{4\pi^2 K^2 \nu x}{UN^2M^2}\right). \tag{16}$$

Taking the square of (16) and averaging with respect to $y$ gives a representation of $u'^2$ by its energy spectrum:

$$\overline{u'^2} = \frac{4\pi^2 q^2}{N^2M^2}\sum_{K=-\infty}^{\infty}\left(\frac{K}{N}\right)^2 |\Delta_K|^2 \exp\left(-\frac{8\pi^2 K^2 \nu x}{UN^2M^2}\right). \tag{17}$$

For $N \to \infty$ the sum in (17) may be replaced by an integral over $k = K/N$ and $|\Delta_K|^2$ by its mean value $|\Delta_K|^2 = N\sigma^2$, because, as a function of $k$, $|\Delta_K|^2$ oscillates rapidly about its mean value and the oscillations do not contribute to the integral.

Writing $K/N = k$ and $(x/M)(\nu/UM) = \bar{x}$, (17) becomes with $N \to \infty$:

$$\overline{u'^2} = \frac{4\pi^2 q^2}{M^2}\sigma^2 \int_{-\infty}^{\infty} k^2 \exp(-8\pi^2 k^2 \bar{x})\,\mathrm{d}k. \tag{18}$$

Equation (18) shows that the spectrum of $\overline{u'^2}$ has a pronounced maximum at $k = 1/(8\pi^2\bar{x})^{\frac{1}{2}}$. The corresponding wavelength is $\lambda = M/k$ or:

$$\lambda/M = (8\pi^2\bar{x})^{\frac{1}{2}}. \tag{19}$$

The fact that the spectrum of $\overline{u'^2}$ has this pronounced peak can explain the rather strange observation that the wake downstream of the screen has an almost sinusoidal velocity distribution (see e.g. figure 3) the wavelength of which increases continually with $\bar{x}$. The theoretical result, equation (19), also shows good quantitative agreement with the observed wavelength, as shown in figures 5 and 7 where (19) is plotted as a solid line.

Equation (18) also allows us to predict the decay of the amplitude $(\overline{u'^2})^{\frac{1}{2}}$ of the velocity disturbance. Performing the integration in (18) and taking the square root gives:

$$(\overline{u'^2})^{\frac{1}{2}} = \frac{2\pi q}{M}\sigma\frac{1}{(8\pi^2\bar{x})^{\frac{3}{4}}}(\tfrac{1}{2}\pi^{\frac{1}{2}})^{\frac{1}{2}} = 0.223\frac{q\sigma}{M}\frac{1}{\bar{x}^{\frac{3}{4}}}. \tag{20}$$

It remains to determine $q/M$ and $\sigma$.

The term $q$ is defined as the integral over the velocity defect profile of a single rod and related to the drag coefficient of the rod. It can, therefore, be related to the pressure loss coefficient $c_D = \Delta p/(\frac{1}{2}\rho)U^2$ of the screen. It is:

$$\frac{q}{UM} \approx \tfrac{1}{4}c_D, \tag{21}$$

and we get: $$\frac{(\overline{u'^2})^{\frac{1}{2}}}{U} = 0.056\,c_D\frac{\sigma}{\bar{x}^{\frac{3}{4}}}. \tag{22}$$

with $\bar{x} = (x/M)(\nu/UM)$.

The standard deviation $\sigma$ of the screens used is not known exactly but its magnitude can be inferred from a technical data sheet of standards for woven screens according to which the permissible average deviation of the mesh width is

$\pm 6\%$. In order to compare the theoretical decay law, equation (22), with observations, experimental $c_D$-values were used. The $c_D$-values can be approximated by $c_D\beta^2/(1-\beta) = 7/(Re_d)^{\frac{1}{3}}$. The standard deviation $\sigma$ was chosen so that a best fit was obtained with the experimental data of figure 6. The velocity amplitude $\Delta U$, plotted in figure 6, is defined as $(U_{\max} - U_{\min})$, which is easier to observe experimentally than $(\overline{u'^2})^{\frac{1}{2}}$. $\Delta U$ was assumed to be, roughly, $\Delta U = 2\sqrt{2}(\overline{u'^2})^{\frac{1}{2}}$, so that:

$$\frac{\Delta U}{U_\infty} = 0.16 c_D \frac{\sigma}{\bar{x}^{\frac{3}{4}}}. \tag{23}$$

Figure 6 shows that a very good agreement with experimental data could be obtained for suitable values of $\sigma$ which are between 3.5% and 6.5% and thus compatible with the cited standards. The theoretical decay law, equation (23), also explains the small additional effect of the Reynolds number $Re_d$ which is displayed by the experimental points and which is theoretically due to the small Reynolds number dependence of the drag coefficient $c_D$.

The above analysis cannot explain that a final wavelength is reached for large values of $x$. It should be noted, however, that the final wavelength is not reached before the amplitude of the disturbances decreases below a few per cent of the free-stream velocity.

## 6. Conclusions

Flow-visualization experiments have led us to the conclusion that the regular pattern of vortices observed in the stagnation region of cylindrical bodies is directly related to the non-uniformities of the oncoming flow and not the result of a stagnation point instability. Moreover, a theoretical analysis could explain why there are fairly regular variations of the streamwise velocity component in the flow downstream of screens. The evolution of the mean wavelength and the decay of the velocity variations agree with the theoretical predictions.

The present investigation is restricted to variations of the streamwise velocity component. For woven screens, due to the three-dimensional nature of the weave, it is expected that variations of the flow direction are also generated by small irregularities of the screen. The spanwise variations in boundary layers observed (e.g. by Bradshaw 1965) have been attributed to such variations of the flow direction in the oncoming flow.

The flow visualization experiments described in §3 of the present paper presuppose that the flow downstream of the screen is steady. For large screen-Reynolds numbers $Ud/\nu$, the flow through the screen becomes turbulent and the unsteady motion will smooth out non-uniformities of the mean flow. It is informative to compare the decay of turbulent fluctuations with the decay of the steady non-uniformities.

According to theoretical studies of Loitsiansky (1939) and Batchelor & Townsend (1948) the energy of homogeneous turbulence decays in the final stage like $u'^2 \sim x^{-\frac{5}{2}}$. In contrast, Birkhoff (1954) and more recently Saffman (1967) conclude that the turbulence energy ultimately decays like $\overline{u'^2} \sim x^{-\frac{3}{2}}$, which agrees with the decay law presently derived for steady non-uniformities, equation (22). The different results follow, basically, from different assumptions about the energy spectrum at low wavenumbers. Loitsiansky's result follows from an energy spectrum that, for $k \to 0$, has the form $E(k) = bk^4 + \ldots$ while Birkhoff's decay law results from an energy spectrum $E(k) = ak^2 + \ldots$.

There are few experimental results on the decay of turbulence in the final period, and it appears that the accuracy of the experimental results is not sufficient to prove one or the other theory. It is possible that the energy spectrum and the decay law depend on the way in which the turbulence was generated initially. A summary of various possible decay laws was given by Rotta (1972). For the steady non-uniformities considered in the present study the energy spectrum for small wavenumbers is $E(k) \sim k^2$ (equation (18)) and consequently the decay law is $\overline{u'^2} \sim x^{-\frac{3}{2}}$. The evolution of the mean wavelength $\lambda \sim x^{\frac{1}{2}}$ agrees with the corresponding law for the turbulence lengthscale.

## REFERENCES


Baines, W. D. & Peterson, E. G. 1951 An investigation of flow through screens. *Trans. ASME* **73**, 467–480.

Batchelor, G. K. & Townsend, A. A. 1948 Decay of turbulence in the final period. *Proc. R. Soc. Lond.* A **194**, 527–543.

Bippes, H. 1972 Experimentelle Untersuchung des laminar-turbulenten Umschlags an einer parallel angeströmten konkaven Wand. *Sitzungsberichte der Heidelberger Akademie der Wissenschaften, mathematisch-naturwissenschaftliche Klasse*. Springer.

Birkhoff, G. 1954 Fourier synthesis of homogeneous turbulence. *Commun. Pure Appl. Maths* **7**, 19–44.

Bohl, J. G. E. von 1940 Das Verhalten paralleler Luftstrahlen. *Ing. Arch.* **11**, 295–314.

Böttcher, J. 1987 Die Strömung im Nachlauf von Sieben und die Entstehung von Längswirbeln in der Staupunktströmung. *DFVLR-FB* 87–27.

Bradshaw, P. 1965 The effect of wind-tunnel screens on nominally two-dimensional boundary layers. *J. Fluid Mech.* **22**, 679–687.

Bray, B. G. de 1967 Some investigations into the spanwise non-uniformity of nominally two-dimensional incompressible boundary layers downstream of gauze screens. *Rep. and Mem. Areo. Res. Council* no. 3578.

Colak-Antic, P. 1971 Visuelle Untersuchungen von Längswirbeln im Staupunktgebiet eines Kreiszylinders bei turbulenter Anströmung. *DLR Mitteilung* 71–13, *Göttingen*, pp. 194–220.

Corrsin, S. 1944 Investigation of the behavior of parallel two-dimensional air jets. *NACA ARC* no. 4H24.

Corrsin, S. 1963 Turbulence: experimental methods. In *Handbuch der Physik* (ed. S. Flügge), vol. 8/2. Springer.

Crow, S. C. 1966 The spanwise perturbation of two-dimensional boundary layers. *J. Fluid Mech.* **24**, 153–164.

Furuya, Y. & Osaka, H. 1975 The spanwise non-uniformity of a nominally two-dimensional turbulent boundary layer. *Bull. JSME* **18**, 664–672.

Görtler, H. 1955 Dreidimensionale Instabilität der ebenen Staupunkströmung gegenüber wirbelartigen Störungen. In *50 Jahre Granzschichtforschung, Vieweg, Braunschweig* (ed. H. Görtler & W. Tollmien), pp. 304–314.

Hainzl, J. 1965 Zur Stabilitätstheorie der Staupunktströmung gegenüber Wirbelstörungen vom Taylor-Görtler-Typ. *DLR-FB* 65–64.

Hämmerlin, G. 1955 Zur Instabilitätstheorie der ebenen Staupunktströmung. In *50 Jahre Grenzschichtforshung, Vieweg, Braunschweig* (ed. H. Görtler & W. Tollmien), pp. 315–327.

Hodson, P. R. & Nagib, H. M. 1975 Longitudinal vortices induced in a stagnation region by wakes – their incipient formation and effects on heat transfer from cylinders. *NASA CR*-152850.

Kestin, J. & Wood, R. T. 1970 On the stability of two-dimensional stagnation flow. *J. Fluid Mech.* **44**, 461–479.

Laws, E. M. & Livesey, J. L. 1978 Flow through screens. *Ann. Rev. Fluid Mech.* **10**, 247–266.

Loitsiansky, L. G. 1939 Some basic laws of isotropic turbulent flow. *Rep. Cent. Aero Hydrodyn. Inst. (Moscow)*, no. 440. (Translated as *Tech. Mem. Natl Adv. Comm. Aero. Wash.* no. 1079).

MEHTA, R. D. 1985 Turbulent boundary layer perturbed by a screen. *AIAA J.* **23**, 1335–1342.

MORGAN, P. G. 1960 The stability of flow through porous screens. *J. Aero. Soc.* **64**, 359–362.

MORKOVIN, M. V. 1979 On the question of instabilities upstream of cylindrical bodies. *NASA Rep.* 3231.

ROTTA, J. C. 1972 *Turbulente Strömungen.* B. G. Teubner, Stuttgart.

SADEH, W. Z., SUTERA, S. P. & MAEDER, P. F. 1970*a* Analysis of vorticity amplification in the flow approaching a two-dimensional stagnation point. *Z. angew. Math. Phys.* **21**, 699–716.

SADEH, W. Z., SUTERA, S. P. & MAEDER, P. F. 1970*b* An investigation of vorticity amplification in stagnation flow. *Z. angew. Math. Phys.* **21**, 717–742.

STAFFMAN, P. G. 1967 The large scale structure of homogeneous turbulence. *J. Fluid Mech.* **27**, 581–593.

SUTERA, S. P. 1965 Vorticity amplification in stagnation-point flow and its effect on heat transfer. *J. Fluid Mech.* **21**, 513–534.

SUTERA, S. P., MAEDER, P. F. & KESTIN, J. 1963 On the sensitivity of heat transfer in stagnation-point boundary layer to free-stream vorticity. *J. Fluid Mech.* **16**, 497–520.

WILSON, S. D. R. & GLADWELL, I. 1978 The stability of a two-dimensional stagnation flow to three-dimensional disturbances. *J. Fluid Mech.* **84**, 517–527.